ACS Photonics

Article

pubs.acs.org/journal/apchd5

Ultrafast Plasmonics on Gold Nanowires: Confinement, Dispersion, and Pulse Propagation

Matthias Wulf, Anouk de Hoogh, Nir Rotenberg, and L. Kuipers*

Center for Nanophotonics, FOM Institute AMOLF, Science Park 104, 1098 XG, Amsterdam, The Netherlands

Supporting Information

ABSTRACT: We explore the potential of plasmonic nanowires for ultrafast photonics by comparing the properties of the guided surface plasmon polariton (SPP) to that of the mode guided in a silicon nanowire. For this purpose, we combine ultrafast near-field microscope measurements of gold nanowires with mode simulations to study modal properties such as mode width, propagation length, fundamental mode cutoff, group velocity dispersion, and third-order dispersion coefficients. Using this information we show that, for ultrashort-pulse propagation, plasmonic waveguides can outperform their dielectric counterparts. In particular, we demonstrate that the ohmic losses, which are unavoidable in the gold nanowire, cause less peak amplitude decay as ultrashort pulses propagate than do the high dispersion and the presence of a mode cutoff.

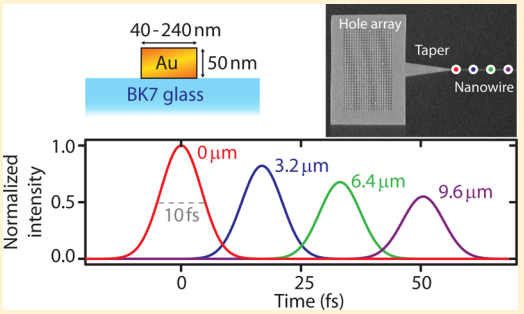

KEYWORDS: *plasmonics, nanowires, pulse propagation, nanophotonic waveguides, near-field microscopy, dispersion*

In the past several years guided plasmonic modes of metallic nanowires (NWs) have emerged as a promising basis for nanophotonic circuits.[1] Interestingly and in stark contrast to conventional dielectric waveguides, decreasing the geometric cross-section of the NWs results in an increased confinement of the plasmonic mode.[2] This increased spatial confinement, which has been demonstrated for various geometries,[3−6] allows for subwavelength guiding[7] and leads to local field enhancements that are beneficial for, for example, nonlinear optics,[8] single-molecule sensing,[9] or strong interaction with quantum emitters.[10] In addition, it has been predicted[11] and experimentally demonstrated[12] that as surface plasmon polaritons (SPPs) are confined, they also slow down. Such a slowdown is beneficial for applications in telecommunication, as it enhances light−matter interactions,[13] allowing for elements with smaller footprints.[14]

Currently, most photonic devices rely on dielectric waveguides, such as ridge or photonic crystal waveguides, rather than plasmonic waveguides.[15−19] These dielectric structures do not suffer from the inherent ohmic losses found in plasmonic materials. Nevertheless, the guided mode of dielectric waveguides does experience geometrical dispersion in addition to the intrinsic material dispersion. In contrast, the dispersion of plasmonic structures is dominated by their material dispersion, and it has been predicted that they can support the broad bandwidth necessary to exhibit sub-femtosecond dynamics.[20,21] In fact, high harmonic generation has been observed when the localized plasmon modes of nanoantennas are driven by femtosecond pulses.[22−24] Further, excitation of metallic nanostructures with femtosecond lasers has enabled studies of their plasmonic resonances.[25,26]

Recent research has raised hopes that plasmonic waveguides might be a viable platform for ultrashort-pulse propagation. Not only have the dispersion relations of various plasmonic waveguides been calculated and measured,[27−29] but pulse propagation on these structures has also been studied.[30−33] From these and other measurements, the group velocities of the different plasmonic modes have been determined[31,34] and even used for spatiotemporal control experiments.[35,36] However, while many of the properties of plasmonic waveguides are known, it remains unclear exactly how ultrashort pulses behave and reshape as they propagate on such structures. More importantly, it remains to be shown whether there are regimes of pulse propagation where plasmonic waveguides can outperform their dielectric counterparts.

In this article we explore ultrashort-pulse propagation on plasmonic nanowires to demonstrate their potential for ultrafast photonics on subwavelength dimensions. We use a series of near-field measurements in conjunction with finite-element method (FEM) calculations to investigate the properties of the plasmonic modes on Au NWs. We then compare these properties of the plasmonic modes to those found on dielectric waveguides. We show that while the plasmonic waveguides outperform their dielectric counterparts in the achievable spatial confinement, the plasmonic mode suffers from a finite propagation length and a lower group index. We demonstrate, however, that the SPP guided in the Au NW experiences much less dispersion than light guided in a Si NW. In particular, the decrease in peak intensity due to temporal pulse reshaping in a dielectric waveguide can be stronger than the decrease due to

Received: July 17, 2014

   dx.doi.org/10.1021/ph500260t | *ACS Photonics* XXXX, XXX, XXX−XXX

the ohmic losses experienced in a plasmonic waveguide, for ultrashort pulses.

We study ultrashort-pulse propagation on plasmonic waveguides by experimentally and theoretically characterizing the properties of lithographically fabricated Au NWs (Figure 1a).

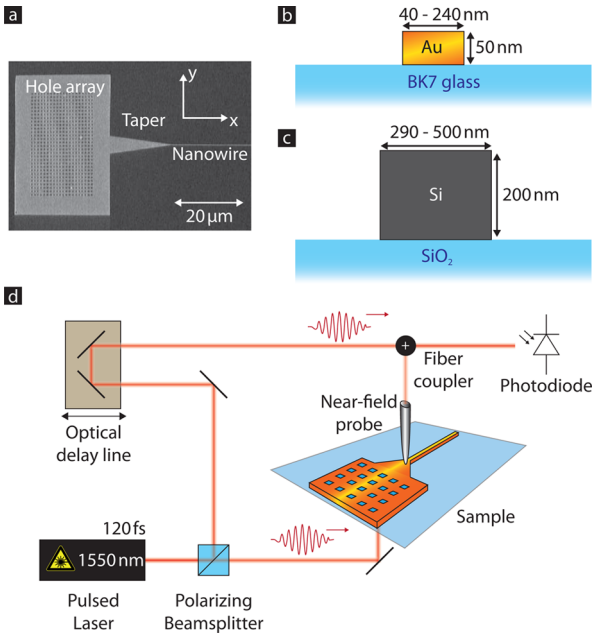

Figure 1. Sample geometry and experimental setup. (a) Micrograph of a typical plasmonic structure consisting of a hole array, a taper, and a nanowire. The hole array and the taper are required to efficiently excite the mode on the Au NW with free-space illumination. Schematic of the cross section of (b) a Au nanowire and (c) a Si nanowire showing the dimensions of the waveguides. (d) Schematic of the home-built near-field scanning optical microscopy setup (NSOM). By integrating an optical delay line and a pulsed laser into an interferometric NSOM we are able to track pulse propagation in Au NWs.

We fix the Au thickness to 50 nm and vary the width between 40 and 240 nm (Figure 1b), where the maximum width is chosen so that our NW is not leaky over the bandwidth of the applied pulsed laser, to determine the geometrically dependent properties of the guided modes. In both the experiments, which are carried out with phase- and time-resolved near-field microscopy[37] (Figure 1d), and the FEM simulations (using the COMSOL multiphysics software package), we study the propagation of telecom (centered at 1550 nm)-wavelength, ultrashort femtosecond pulses. Experimentally, we excite SPPs by illuminating a hole array, whose periodicity has been carefully selected to resonantly couple free-space radiation to plasmons on the Au−glass interface and not on the Au−air interface, with a laser.[38] These interface SPPs are then adiabatically funneled with a taper into NW plasmons.[2] We map the near-fields of the guided mode using our near-field microscope. In these measurements we use a 250 nm aperture probe, which delivers a good trade-off between the signal-to-noise ratio and the optical resolution. For the simulations, the dispersive material refractive index of Au is taken from the literature,[39] and the refractive index of the BK7 glass substrate (of our samples) is fixed at 1.5. More details about the experimental and simulation procedures are provided in the Supporting Information.

One of the fundamental advantages of plasmonic waveguides, over dielectrics, is that they are expected to very strongly confine light to the waveguiding region. Consequently, we begin by investigating the spatial confinement of the plasmonic modes. We measure the in-plane field amplitude and phase of the guided SPPs in the NW, using CW illumination. Consequently, we are able to Fourier filter[40] our signal and create the in-plane intensity maps of the SPPs, an example of which is shown in Figure 2a for a 240 nm wide NW. Here, we

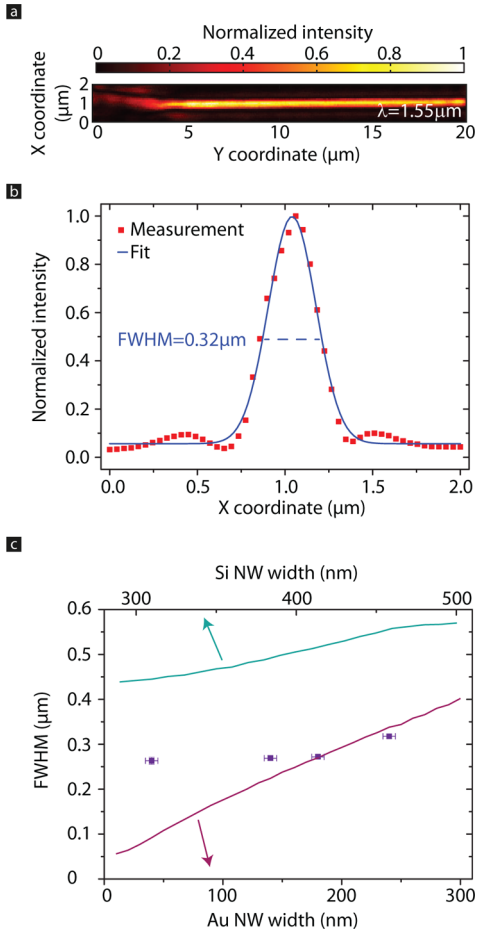

Figure 2. Mode width of the NWs at a wavelength of 1.55 μm. (a) Measured spatial intensity map of an SPP propagating on a 240 nm wide Au NW with CW laser excitation. The funneling of the SPPs from the taper at the left to the nanowire on the right is observed. (b) Cross-cut in the x-direction after normalizing and averaging the NW intensity profile of (a) and a corresponding Gaussian fit. The SPP guided by the Au NW has a mode width of 0.32 μm. (c) Dependence of the mode width on the NW width for the Au NW (measurements shown by symbols and simulations by the purple curve) and the Si NW (cyan curve). A decrease of the mode width with decreasing NW width can be observed. The plasmonic structure exhibits a stronger spatial confinement than the dielectric waveguide.

see how an SPP propagating from the left is funneled from the taper into the NW (starting around $y = 7$ μm). For a wide taper width, an electric field can only be observed at the edges of the Au layer. As the taper width narrows, the electric field of the SPP "wraps around" the NW, and consequently we can detect a signal above the NW. In fact, we measure the highest intensity at the beginning of the NW, which then decays with propagation due to the ohmic losses of the SPP. We can

dx.doi.org/10.1021/ph500260t | ACS Photonics XXXX, XXX, XXX−XXX

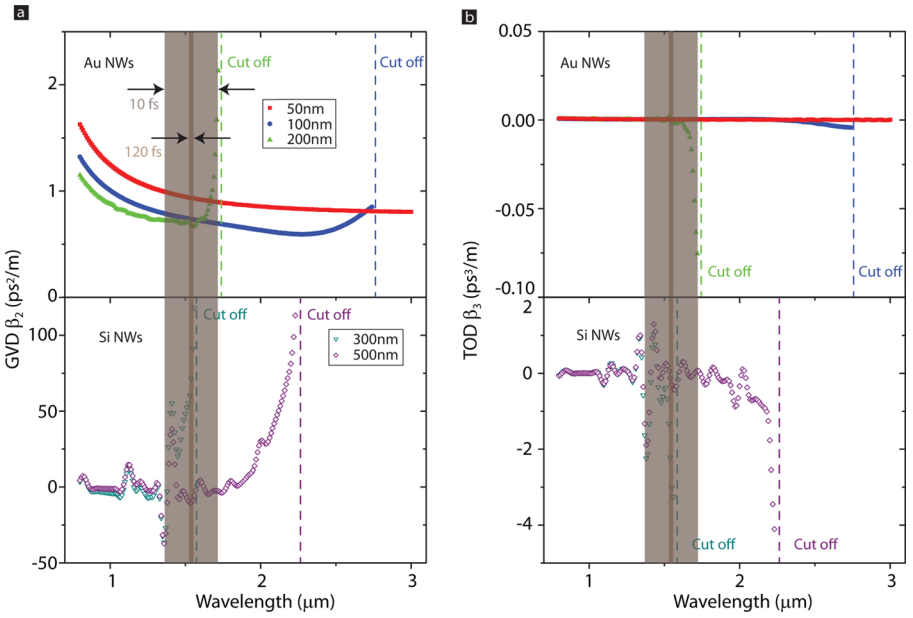

Figure 3. Dispersion properties of Au and Si NWs. (a) The GVD coefficient as a function of wavelength. (b) The TOD coefficient as a function of wavelength. Top panel: Au NWs. Bottom panel: Si NWs. The plasmonic waveguides feature 2 orders of magnitude smaller GVD and TOD coefficients than do the Si NWs. Dashed lines indicate the cutoff wavelengths of the correspondent modes. The shaded areas represent the spectral region populated by the fwhm bandwidth of a 10 and 120 fs pulse, respectively. The oscillations, which can be seen on top of the GVD and TOD curves of the Si NWs, are numerical artifacts from the FEM simulation and do not have a physical origin.

quantify the spatial confinement of the mode by averaging intensity cross-cuts in the x-direction along the nanowire and fitting a Gaussian function to this averaged cross-cut (Figure 2b). More details about how the mode width is extracted from the near-field measurements can be found in the Supporting Information. We repeat this fitting procedure for different nanowire widths to determine the dependence of the mode width on the NW cross-section. The results of these measurements are depicted as squares in Figure 2c. As expected, we observe that the mode width decreases, and hence the confinement increases, as the NW cross-section decreases. Here, the horizontal error bars (±5 nm) are due to uncertainties in the determination of the NW width, while our uncertainty in the fwhm (~10 nm) is too small to be visible in Figure 2c.

This trend of increasing confinement for smaller NWs is reproduced by the simulations (solid curve in Figure 2c). There is, however, a deviation between the simulated and measured mode widths, particularly for smaller NWs. This discrepancy can be explained by the finite aperture size of the near-field probe used in the experiment, which limits the smallest measurable fwhm values. Since we use a probe with a 250 nm aperture, for small NW widths the measured mode width represents the aperture size, while for larger widths we measure values close to the actual lateral field spread. The nearly monotonic decrease of the mode width with NW dimensions observed in the simulations confirms that the SPP can be guided on arbitrary small plasmonic waveguides.

Having established how the plasmonic NWs confine light, we turn to the dielectric waveguides and look for a geometry where similar confinement occurs. Specifically, we want to compare the plasmonic NW to a ubiquitous dielectric NW, the Si NW[15,41−46] (Figure 1c). We fix the height of the Si NW to 200 nm and allow the width to range between 290 and 500 nm. The smallest width of 290 nm is chosen since smaller Si NWs no longer support a guided mode[47] (see Supporting Information). The dispersive refractive indices of the Si core and the silica substrate are taken from the literature.[48,49] Since these dielectric waveguides have been extensively studied,[50−52] we limit ourselves to simulations of their properties, investigating only the Au NWs experimentally.

The simulated mode width of the Si NWs, which we show with a cyan curve in Figure 2c, qualitatively behaves in much the same way as the mode width of the Au NWs: the width of the mode decreases with the NW width. There are, however, a few important differences to note between the behavior of the dielectric and plasmonic waveguides. First, the mode of the Si NW is always wider than that of the Au NW. Further, whereas the mode width for the plasmonic waveguide is, in principle, not restricted to a minimum value, we find a minimum mode width for the dielectric waveguide of ~430 nm. This suggests that, if we want to compare plasmonic and dielectric waveguides with similar light confinement, we should use the narrowest Si NW available. Consequently, we will mainly consider a 300 nm wide Si NW hereafter, although we note that the mode width of this NW is still 2.0 and 1.1 times larger than that of a 140 or 300 nm Au NW, respectively.

Having found that the plasmonic and dielectric NWs can confine light to similar dimensions, we set out to determine the differences and similarities of pulse propagation on these structures. An important quantity that describes the evolution of a propagating pulse in a waveguide is the dispersion relation $k(\omega)$.[53] The first derivative of the dispersion relation with respect to frequency is related to the group velocity of the pulse and describes the temporal shift of the pulse envelope with propagation. The second and third derivatives of $k(\omega)$, which quantify the group velocity dispersion (GVD) and third-order dispersion (TOD), respectively, are the most important dispersion properties of the waveguide since they specify the strongest contributions to the temporal pulse reshaping during propagation. GVD causes a symmetrical temporal broadening of the pulse envelope, whereas TOD leads to an asymmetrical

dx.doi.org/10.1021/ph500260t | ACS Photonics XXXX, XXX, XXX−XXX

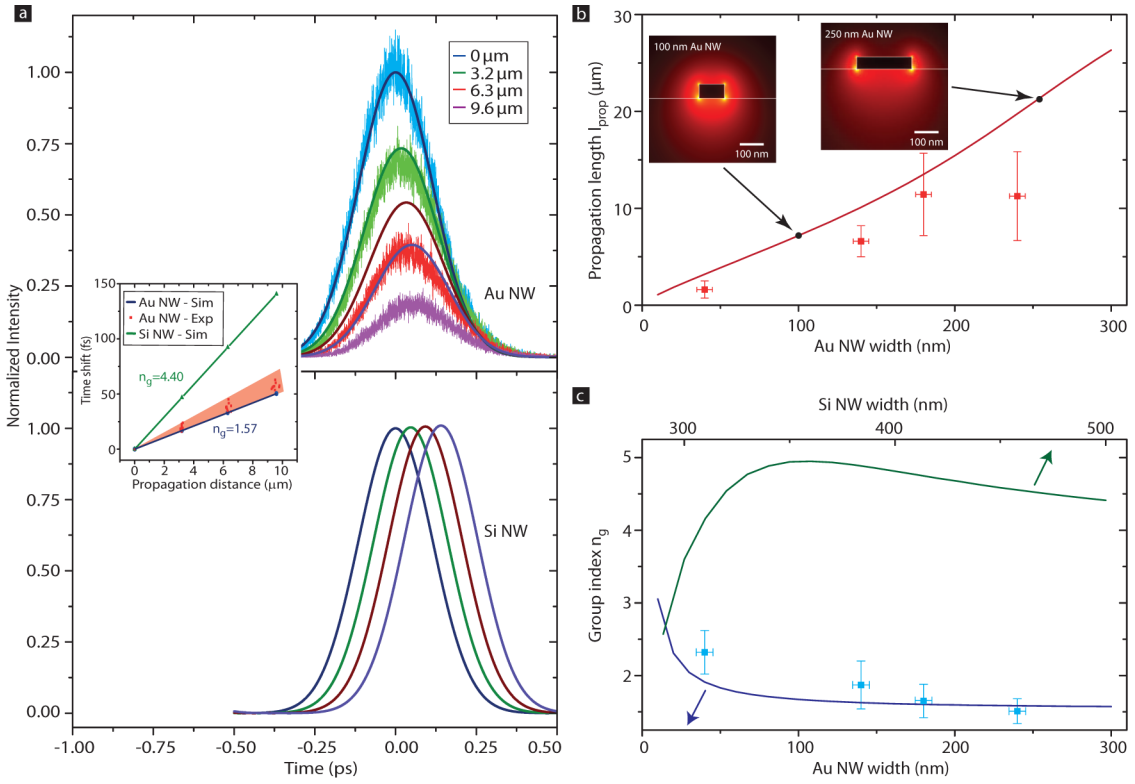

Figure 4. Temporal dynamics of a 120 fs pulse propagating in Au and Si NWs. (a) Top panel: A comparison between a typical measurement series (thick curves) at different locations along a Au NW (width = 140 nm) and a semianalytical calculation of the pulse propagation (thin curves). The inset shows the arrival time with propagation and gives the group indices. Bottom panel: An analytical calculation of pulse propagation inside a Si NW (width = 300 nm). The curves are normalized to the maximum intensity at a propagation distance of 0 μm. Measured (squares) and simulated (curve) dependence of (b) the propagation length and (c) the group index on the nanowire width. Note that, at 1550 nm, the Si NW is ideally lossless and hence has an $l_{prop} = \infty$. The insets in (b) show the electric field distribution of the mode guided along a 100 nm and a 250 nm wide Au NW, respectively.

broadening. In Figure 3 both quantities, calculated from the simulated dispersion relation for several NW geometries (see Supporting Information for more information), are shown as a function of wavelength.

In general, Figure 3 shows how changing the geometry affects the dispersion of the plasmonic and dielectric waveguides. The amplitude of the dispersion coefficients is increased when the NW sizes are decreased, at all wavelengths. In the case of the Au NWs, the GVD and TOD increase when the NW width is narrowed. In addition, there is a cutoff, i.e., a wavelength above which a guided mode becomes leaky, for the two wider Au NWs. In contrast, for the dielectric waveguides the dispersion curves shift to shorter wavelengths when the NW width is decreased. As a consequence, the spectral regime of high dispersion, close to the cutoff, is blue-shifted. For example, the cutoff shifts from 2.25 to 1.6 μm when the NW width is decreased from 500 to 300 nm. The amplitude of GVD and TOD can be compared between Au and Si NWs. Most importantly, we see that the dispersion coefficients for the Si NWs are an order of magnitude larger than for their plasmonic counterparts. This huge difference in the amplitude of GVD and TOD shows that the dielectric waveguides are intrinsically more dispersive than the Au NWs, especially when operated close to the cutoff of the guided mode, where the dispersion coefficients diverge. Note that the oscillations on top of the GVD and TOD curves of the Si NW are numerical artifacts from the FEM simulations and do not have a physical origin.

To experimentally investigate ultrashort-pulse propagation and to check if the superior dispersion properties of the plasmonic NWs are observable in experiment, we perform time-resolved measurements on the Au NWs using 120 fs long pulses. With our near-field microscope[54] we collect field transients at different positions along the plasmonic waveguide (see Supporting Information for more details). In Figure 4a, which presents an exemplary measurement on a 140 nm wide Au NW, we present the temporal evolution of a pulse during propagation. Here, we positioned the near-field probed at four different propagation distances in the first 10 μm along the plasmonic structure and scanned the optical delay line to extract the temporal pulse envelope at these locations. In general, a Gaussian wave packet (fwhm of 120 fs) is observed, which decays in intensity and moves in time, as the propagation distance increases. When moving 9.6 μm along the Au NW, the intensity decreases by 85% and the wave packet shifts by 60 fs.

To understand the temporal evolution of the pulse envelope, we compare the measurement to the result of a semianalytical calculation of the pulse propagation (thin curves). In the calculation we solve the one-dimensional wave equation in the spectral domain:[53]

$$\frac{\partial \hat{A}(z, \omega)}{\partial z} = iK(\omega)\,\hat{A}(z, \omega) \tag{1}$$

where $\hat{A}(z, \omega)$ and $K(\omega)$ are the spectral density of the pulse and the frequency-dependent complex wavenumber, respectively. This equation takes the linear absorption and dispersion

dx.doi.org/10.1021/ph500260t | ACS Photonics XXXX, XXX, XXX−XXX

that occur during pulse propagation into account (see Supporting Information for more details). There is good agreement between the experiment and the semianalytical calculation (thick and thin curves in Figure 4a). The temporal movement of the wave packet is well reproduced, and only a small discrepancy in the intensity decay is observed. The experiment shows a slightly faster decay than the calculation.

We use the time-resolved near-field measurements to quantify both the losses and the speed at which a pulse propagates along the NW. The intensity decay with propagation is reproduced well by an exponential fit to the envelope amplitude, which yields the propagation length, l_{prop}. The increase in arrival time contains information about the group delay and can be used to extract the group velocity (v_g) and the group index ($n_g = c/v_g$), respectively, provided that no significant reshaping of the pulse envelope occurs (cf. inset in Figure 4a).

The propagation loss, in the plasmonic NW, is due to ohmic losses, namely, the conversion of electromagnetic energy to heat as light is absorbed by the free electrons of the Au. Since the mode properties, such as the loss, are dependent on the width of the NW, we again investigate different NW geometries. Figure 4b summarizes the extracted propagation length of several temporal near-field measurements. In this figure, each symbol is the average l_{prop} from each series of measurements, while the error bars are given by the corresponding variance. Indeed, we observe that the propagation length increases with increasing NW dimensions, as less field is confined to the metal (see insets of the modal field profiles in Figure 4b). These observations are in good agreement with our simulations, although the measured propagation lengths are slightly smaller than the simulated values, indicative of an additional loss channel such as scattering from imperfections, which is not taken into account in the FEM simulation. Further, the measurements and simulations diverge for the largest NWs (width of ~240 nm). Although such a deviation has been previously observed,[2] its exact cause remains unclear. It is, however, likely that leakage radiation losses into the substrate, which are known to occur for wider NWs, play a role.

We now turn to the speed at which the pulses propagate through the waveguides, which can be characterized by the group index of the mode. This parameter can be extracted by fitting a straight line to the linear time shift with propagation distance observed for the pulse in the experiment (cf. inset in Figure 4a). Figure 4c shows a comparison of the measured and simulated group index for Au NWs of different widths, where the values and vertical error bars are again extracted from a statistical analysis of several measurements on each nanowire. In general, we observe the expected trend that smaller Au NW widths lead to slower SPPs,[11,31] with excellent agreement between experiments and simulations. The highest n_g value of 2.32 is measured for the narrowest width of 40 nm, and the simulation shows that this trend continues even further with decreasing NW width. These results show that there is a trade-off to be made in plasmonic waveguides: either there is a large slowdown combined with a huge spatial confinement and high losses, or less slowdown is achieved with a smaller confinement but also fewer losses.

Next, we compare the propagation of a 120 fs pulse on Si NWs with our observations for the plasmonic structures. From the FEM simulations we again extract l_{prop} and n_g for the different NW widths, as was done for the Au NWs. In fact, at 1550 nm, Si NWs that support a guided mode are, ideally, lossless, and hence $l_{prop} = \infty$ for all widths. In contrast, n_g shows a rich width dependence. First, the group index increases with increasing NW width until it reaches a maximum of ~4.95 for a width of ~360 nm. Increasing the NW width further causes the group index to decrease again. Additionally, the mode guided in the Si NW is nearly always 2 to 3 times slower than an SPP propagating in a Au NW. This situation changes only for extremely small Au NW cross-sections.

As with plasmonic NWs, we can use the results of our simulations of the Si NW modes to semianalytically calculate how 120 fs pulses would propagate on these structures. In the bottom panel of Figure 4a we show the results of such a calculation, in this case for a 300 nm wide NW. In contrast to the plasmonic structure (top panel), we observe that, in the Si NW, the pulses both propagate more slowly and experience no loss. That is, other than a slightly weaker confinement, the Si NW appears to outperform the Au NW when 120 fs long pulses are considered.

In our measurements of the 120 fs pulses propagation on the Au NWs (Figure 4a) we observe no reshaping of the pulse envelope. This suggests that within the 30 nm bandwidth of the pulse spectrum, dispersion is negligible. That is, the different spectral components that make up the pulse all travel at a similar group velocity, and hence the pulse envelope is relatively unchanged during propagation. Likewise, our semianalytic modeling of pulse propagation in the Si NWs, which uses the dispersion relation determined by simulations, shows that for this 30 nm bandwidth dispersion is also negligible for the dielectric waveguide. This fact can also be quantified by calculating the dispersion length, i.e., the propagation distance after which the temporal pulse width is broadened by a factor $\sqrt{2}$ (see more information in the Supporting Information). For a pulse duration of 120 fs, all geometries feature a dispersion length that is much longer than 10 μm. Consequently, no temporal reshaping is visible.

The temporal reshaping of pulses does not depend only on the amplitude of the dispersion coefficients, but also on the bandwidth of the pulse. It therefore remains to be seen how broad bandwidth pulses evolve as they propagate on Au and Si NWs. Consequently, we investigate the propagation of 10 fs pulses, which have a spectral bandwidth of 350 nm as compared to the 30 nm bandwidth of the 120 fs pulses. We note that 10 fs pulses, at 1550 nm, span only two optical cycles and are therefore among the shortest possible pulses at this wavelength. As can be seen in Figure 3, for the broad range of wavelengths contained within these short pulses the dispersion relation is far from flat. The dispersion length of the 10 fs pulses propagating on the narrow Si NW is smaller than 10 μm, whereas it is still several tens of micrometers long for the other NW geometries. Hence, temporal reshaping due to dispersion should be visible in the 300 nm wide dielectric waveguide, whereas the shape of the envelope should remain unchanged for the other NWs.

Figure 5 presents the results of the semianalytical calculations performed for a pulse duration of 10 fs. It is obvious that the pulse envelope does not reshape while propagating through the plasmonic waveguides. Only the amplitude of the pulse drops due to the ohmic losses. In contrast, there is significant reshaping visible in the case of the 300 nm wide Si NW. Here, the Gaussian wave packet collapses into two peaks, which propagate with different group velocities and therefore separate in time with increasing propagation distance. This behavior can be explained by looking at the dispersion relation of this

dx.doi.org/10.1021/ph500260t | ACS Photonics XXXX, XXX, XXX−XXX

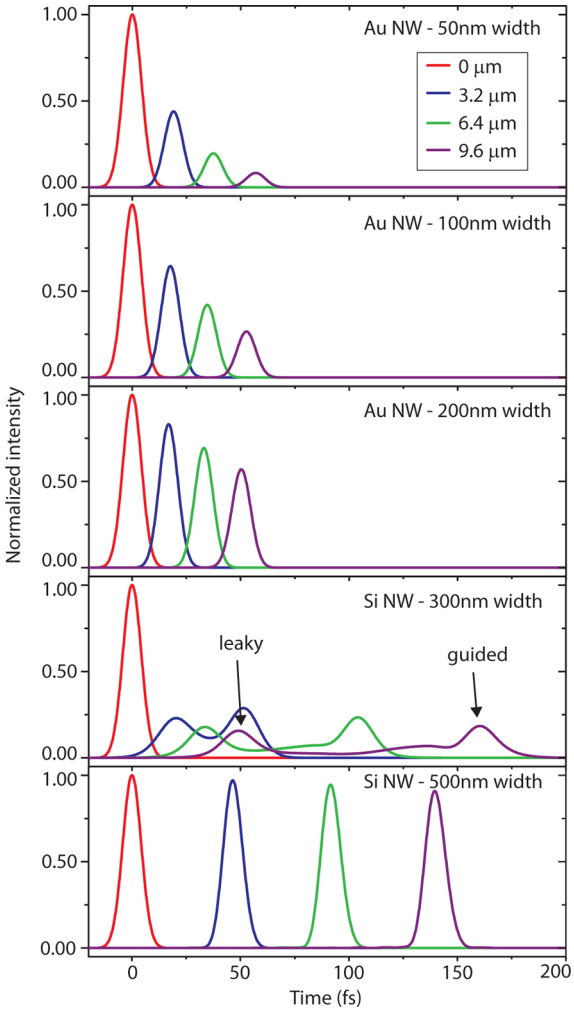

Figure 5. Propagation of a 10 fs short pulse on the various NWs. The pulse shows no temporal reshaping in the plasmonic waveguide; only an intensity decay due to ohmic losses is visible. In contrast, in the 300 nm wide Si NW the pulse envelope is distorted due to strong dispersion and the proximity of the mode cutoff. For a 500 nm wide Si NW the guided mode experiences much less dispersion and its bandwidth does not cross the mode cutoff. Consequently the 10 fs pulse does not temporally reshape. Note that the 500 nm wide Si NW supports two modes at this wavelength, and hence its applicability is limited. All curves are normalized to the maximum intensity of the pulse at a propagation distance of 0 μm.

dielectric waveguide. The fundamental mode has a cutoff wavelength of 1600 nm, and the spectral bandwidth of the pulse is so broad that part of the energy populates also the frequency regime where the mode is leaky (more information can be found in the Supporting Information). Thus, the slowly moving peak, which reshapes with propagation due to dispersion, represents the frequency components in the guided regime, whereas the fast moving peak is built up by the spectral components in the leaky regime. A detailed discussion of the contributions to the temporal reshaping is contained in the Supporting Information. This explanation can also be translated to the wider Si NW to understand why this waveguide does not show temporal reshaping of the pulse. Here, the cutoff wavelength, and therefore the highly dispersive regime, is red-shifted to longer wavelengths. Since the spectral bandwidth of the pulse is not large enough so that its spectral density covers the shifted cutoff, no dispersion is visible in the 500 nm wide dielectric waveguide. However, please note that this Si NW has limited application prospects, as it supports multiple modes at a wavelength of 1.55 μm. These observations of the pulse reshaping confirm that for few-cycle femtosecond pulses in high confinement waveguides, Au NWs display superior properties. In general, high-confinement plasmonic waveguides do not show a cutoff for the guided SPP and, hence, can be used in a broad spectral range without becoming multimode (see Supporting Information). Second, the Au NWs are much less dispersive than Si NWs.

Another important feature to consider for pulse propagation applications is the decay behavior of the peak intensity for the various geometries. The peak intensity of a pulse is crucial for applications such as nonlinear optics and contains information about the temporal reshaping during propagation. In contrast to what we observed for the longer pulses, Figure 5 shows that the peak intensity of a 10 fs pulse in the wider Au NW decreases more slowly than in the narrow Si NW. In detail, in the 100 nm wide plasmonic NW the peak intensity drops to 64% of its starting value after a propagation of 3.2 μm, whereas it decreases to 29% in the case of the 300 nm wide dielectric waveguide. The higher peak intensity of the plasmonic mode persists also for longer propagation distances up to 9.6 μm. This advantageous difference, which comes from the drastic temporal reshaping that the pulse undergoes in the Si NW, can be even further increased by using a wider Au NW. Such wide Au NWs are less lossy, albeit at the cost of decreased spatial confinement, although they still feature a smaller mode width than the Si NWs. Thus, the plasmonic waveguides outperform their dielectric waveguides in the case of few cycle pulse propagation if a high spatial confinement and less temporal reshaping are needed.

In conclusion, we demonstrated that Au NWs are promising candidates for applications where high-field confinements and ultrashort pulse propagation are desired. We experimentally confirmed that light can be confined in smaller areas in Au NWs than in Si NWs. In addition, we show that the low dispersion and the absence of a mode cutoff in plasmonic waveguides can outweigh the inherent ohmic losses, which are absent in their dielectric counterparts, if the applied pulse is as short as 10 fs.

While we have compared the performance of plasmonic waveguides with those that are composed purely of dielectrics, there are, of course, also waveguides composed of both metal and dielectric parts. For example, dielectric-loaded plasmonic waveguides (DLSPPW) consist of a dielectric strip on top of a metallic layer. The modal properties of dielectric-loaded plasmonic waveguides have been thoroughly investigated in the literature[28,55] and, as can be expected, lie in between those of the pure plasmonic and dielectric waveguides. For example, a narrow dielectric strip on a metal surface will act almost like a pure dielectric waveguide, while if the strip is widened, then its modes will become increasingly plasmonic. Consequently, for these dielectric-loaded plasmonic waveguides, there is an inherent trade-off between propagation length and mode confinement, where the prior decreases and the latter increases as the mode becomes more plasmonic. Similarly, the group velocity dispersion of the mode guided in the DLSPPWs, which was found to be on average 10 ps^2/m,[28] lies between the group velocity dispersions that we find for the pure waveguides. There are also more complicated waveguide structures like hybrid plasmonic waveguides,[5,6] which feature superior modal properties, i.e., better confinement and longer propagation lengths.

dx.doi.org/10.1021/ph500260t | ACS Photonics XXXX, XXX, XXX−XXX

While the dispersion in these structures is largely unknown, it is beyond the scope of this paper.

The results presented in this paper reveal the potential of Au NWs for ultrafast photonics on the nanometer scale. For example, the slow decay of the peak intensity of the SPP guided in Au NWs in comparison to the mode in Si NWs will be beneficial for nonlinear optics. Likewise, the negligible temporal reshaping in the plasmonic waveguides can be instrumental to implement short-range ultrafast optical communication systems.

■ ASSOCIATED CONTENT

Supporting Information

More details about the near-field microscopy measurements, the Drude model and the approach to extract dispersion from the FEM mode simulations, the dependence of the real part of the effective mode index on the NW width, the single-mode operation of the NWs, the effect of using different material data sets for gold, the semianalytical pulse propagation calculations, and the dispersion length. This material is available free of charge via the Internet at http://pubs.acs.org.

■ AUTHOR INFORMATION

Corresponding Author

*E-mail: kuipers@amolf.nl.

Notes

The authors declare no competing financial interest.

■ ACKNOWLEDGMENTS

This work is part of the research programme of the Foundation for Fundamental Research on Matter (FOM), which is part of the Netherlands Organisation for Scientific Research (NWO). This work was also funded by an ERC Advanced Investigator Grant (no. 240438 - CONSTANS). We would like to acknowledge funding from the European Union (Project SPANGL4Q) and NanoNextNL, a micro- and nanotechnology consortium of the Government of The Netherlands and 130 partners. We thank Hinco Schoenmaker for technical support.

■ REFERENCES

(1) Gramotnev, D. K.; Bozhevolnyi, S. I. Plasmonics beyond the diffraction limit. *Nat. Photonics* **2010**, *4*, 83−91.

(2) Verhagen, E.; Spasenović, M.; Polman, A.; Kuipers, L. Nanowire plasmon excitation by adiabatic mode transformation. *Phys. Rev. Lett.* **2009**, *102*, 203904.

(3) Bozhevolnyi, S. I.; Volkov, V. S.; Devaux, E.; Ebbesen, T. W. Channel plasmon-polariton guiding by subwavelength metal grooves. *Phys. Rev. Lett.* **2005**, *95*, 046802.

(4) Moreno, E.; Rodrigo, S. G.; Bozhevolnyi, S. I.; Martín-Moreno, L.; García-Vidal, F. J. Guiding and Focusing of Electromagnetic Fields with Wedge Plasmon Polaritons. *Phys. Rev. Lett.* **2008**, *100*, 023901.

(5) Oulton, R. F.; Sorger, V. J.; Genov, D. A.; Pile, D. F. P.; Zhang, X. A hybrid plasmonic waveguide for subwavelength confinement and long-range propagation. *Nat. Photonics* **2008**, *2*, 496−500.

(6) Sorger, V. J.; Ye, Z.; Oulton, R. F.; Wang, Y.; Bartal, G.; Yin, X.; Zhang, X. Experimental demonstration of low-loss optical waveguiding at deep sub-wavelength scales. *Nat. Commun.* **2011**, *2*, 331.

(7) Ditlbacher, H.; Hohenau, A.; Wagner, D.; Kreibig, U.; Rogers, M.; Hofer, F.; Aussenegg, F. R.; Krenn, J. R. Silver nanowires as surface plasmon resonators. *Phys. Rev. Lett.* **2005**, *95*, 257403.

(8) Bouhelier, A.; Beversluis, M.; Hartschuh, A.; Novotny, L. Near-field second-harmonic generation induced by local field enhancement. *Phys. Rev. Lett.* **2003**, *90*, 013903.

(9) Nie, S.; Emory, S. R. Probing single molecules and single nanoparticles by surface-enhanced Raman scattering. *Science* **1997**, *275*, 1102−1106.

(10) Akimov, A. V.; Mukherjee, A.; Yu, C. L.; Chang, D. E.; Zibrov, A. S.; Hemmer, P. R.; Park, H.; Lukin, M. D. Generation of single optical plasmons in metallic nanowires coupled to quantum dots. *Nature* **2007**, *450*, 402−406.

(11) Stockman, M. I. Nanofocusing of optical energy in tapered plasmonic waveguides. *Phys. Rev. Lett.* **2004**, *93*, 137404.

(12) Kravtsov, V.; Atkin, J. M.; Raschke, M. B. Group delay and dispersion in adiabatic plasmonic nanofocusing. *Opt. Lett.* **2013**, *38*, 1322−1324.

(13) Krauss, T. F. Why do we need slow light? *Nat. Photonics* **2008**, *2*, 448−450.

(14) Baba, T. Slow light in photonic crystals. *Nat. Photonics* **2008**, *2*, 465−473.

(15) Jalali, B.; Fathpour, S. Silicon photonics. *J. Lightwave Technol.* **2006**, *24*, 4600−4615.

(16) Saleh, B. E. A.; Teich, M. C. *Fundamentals of Photonics*; Wiley-Interscience, 2007.

(17) Hunsperger, R. G. *Integrated Optics: Theory and Technology*; Springer, 2009.

(18) Pollock, C. R.; Lipson, M. *Integrated Photonics*; Kluwer Academic Publishers, 2003.

(19) Asghari, M.; Krishnamoorthy, A. V. Silicon photonics: energy-efficient communication. *Nat. Photonics* **2011**, *5*, 268−270.

(20) Stockman, M. I.; Kling, M. F.; Kleineberg, U.; Krausz, F. Attosecond nanoplasmonicfield microscope. *Nat. Photonics* **2007**, *1*, 539−544.

(21) Stockman, M. I. Nanoplasmonics: past, present, and glimpse into future. *Opt. Express* **2011**, *19*, 22029−22106.

(22) Kim, S.; Jin, J.; Kim, Y.-J.; Park, I.-Y.; Kim, Y.; Kim, S.-W. High-harmonic generation by resonant plasmon field enhancement. *Nature* **2008**, *453*, 757−760.

(23) Hanke, T.; Krauss, G.; Träutlein, D.; Wild, B.; Bratschitsch, R.; Leitenstorfer, A. Efficient nonlinear light emission of single gold optical antennas driven by few-cycle near-infrared pulses. *Phys. Rev. Lett.* **2009**, *103*, 257404.

(24) Sivis, M.; Duwe, M.; Abel, B.; Ropers, C. Extreme-ultraviolet light generation in plasmonic nanostructures. *Nat. Phys.* **2013**, *9*, 304−309.

(25) Douillard, L.; Charra, F.; Korczak, Z.; Bachelot, R.; Kostcheev, S.; Lerondel, G.; Adam, P.-M.; Royer, P. Short range plasmon resonators probed by photoemission electron microscopy. *Nano Lett.* **2008**, *8*, 935−940.

(26) Hrelescu, C.; Sau, T. K.; Rogach, A. L.; Jäckel, F.; Laurent, G.; Douillard, L.; Charra, F. Selective excitation of individual hotspots at the tips of single gold nanostars. *Nano Lett.* **2011**, *11*, 402−407.

(27) Moreno, E.; García-Vidal, F. J.; Rodrigo, S. G.; Martin-Moreno, L.; Bozhevolnyi, S. I. Channel plasmon-polaritons: modal shape, dispersion, and losses. *Opt. Lett.* **2006**, *31*, 3447−3449.

(28) Krasavin, A. V.; Zayats, A. V. Silicon-based plasmonic waveguides. *Opt. Express* **2010**, *18*, 11791−11799.

(29) Leißner, T.; Lemke, C.; Fiutowski, J.; Radke, J. W.; Klick, A.; Tavares, L.; Kjelstrup-Hansen, J.; Rubahn, H.-G.; Bauer, M. Morphological tuning of the plasmon dispersion relation in dielectric-loaded nanofiber waveguides. *Phys. Rev. Lett.* **2013**, *111*, 046802.

(30) Sandtke, M.; Kuipers, L. Slow guided surface plasmons at telecom frequencies. *Nat. Photonics* **2007**, *1*, 573−576.

(31) Rewitz, C.; Keitzl, T.; Tuchscherer, P.; Huang, J.-S.; Geisler, P.; Razinskas, G.; Hecht, B.; Brixner, T. Ultrafast plasmon propagation in nanowires characterized by far-field spectral interferometry. *Nano Lett.* **2012**, *12*, 45−49.

(32) Kubo, A.; Pontius, N.; Petek, H. Femtosecond microscopy of surface plasmon polariton wave packet evolution at the silver/vacuum interface. *Nano Lett.* **2007**, *7*, 470−475.

(33) Lemke, C.; Leißner, T.; Klick, A.; Fiutowski, J.; Radke, J. W.; Thomaschewski, M.; Kjelstrup-Hansen, J.; Rubahn, H.-G.; Bauer, M.

The complex dispersion relation of surface plasmon polaritons at gold/para-hexaphenylene interfaces. *Appl. Phys. B: Laser Opt.* **2014**, *116*, 585−591.
(34) Geisler, P.; Razinskas, G.; Krauss, E.; Wu, X.-F.; Rewitz, C.; Tuchscherer, P.; Goetz, S.; Huang, C.-B.; Brixner, T.; Hecht, B. Multimode plasmon excitation and in situ analysis in top-down fabricated nanocircuits. *Phys. Rev. Lett.* **2013**, *111*, 183901.
(35) Huang, J. S.; Voronine, D. V.; Tuchscherer, P.; Brixner, T.; Hecht, B. Deterministic spatiotemporal control of optical fields in nanoantennas and plasmonic circuits. *Phys. Rev. B* **2009**, *79*, 195441.
(36) Rewitz, C.; Razinskas, G.; Geisler, P.; Krauss, E.; Goetz, S.; Pawłowska, M.; Hecht, B.; Brixner, T. Coherent control of plasmon propagation in a nanocircuit. *Phys. Rev. Appl.* **2014**, *1*, 014007.
(37) Sandtke, M.; Engelen, R. J. P.; Schoenmaker, H.; Attema, I.; Dekker, H.; Cerjak, I.; Korterik, J. P.; Segerink, F. B.; Kuipers, L. Novel instrument for surface plasmon polariton tracking in space and time. *Rev. Sci. Instrum.* **2008**, *79*, 013704.
(38) Devaux, E.; Ebbesen, T. W.; Weeber, J.-C.; Dereux, A. Launching and decoupling surface plasmons via micro-gratings. *Appl. Phys. Lett.* **2003**, *83*, 4936−4938.
(39) Johnson, P. B.; Christy, R. W. Optical constants of the noble metals. *Phys. Rev. B* **1972**, *6*, 4370−4379.
(40) Gersen, H.; Karle, T. J.; Engelen, R. J. P.; Bogaerts, W.; Korterik, J. P.; van Hulst, N. F.; Krauss, T. F.; Kuipers, L. Direct observation of Bloch harmonics and negative phase velocity in photonic crystal waveguides. *Phys. Rev. Lett.* **2005**, *94*, 123901.
(41) Bogaerts, W.; Baets, R.; Dumon, P.; Wiaux, V.; Beckx, S.; Taillaert, D.; Luyssaert, B.; Van Campenhout, J.; Bienstman, P.; Van Thourhout, D. Nanophotonic waveguides in silicon-on-insulator fabricated with CMOS technology. *J. Lightwave Technol.* **2005**, *23*, 401−412.
(42) Xia, F.; Sekaric, L.; Vlasov, Y. Ultracompact optical buffers on a silicon chip. *Nat. Photonics* **2007**, *1*, 65−71.
(43) Osgood, R. M., Jr.; Panoiu, N. C.; Dadap, J. I.; Liu, X.; Chen, X.; Hsieh, I.-W.; Dulkeith, E.; Green, W. M. J.; Vlasov, Y. A. Engineering nonlinearities in nanoscale optical systems: physics and applications in dispersion-engineered silicon nanophotonic wires. *Adv. Opt. Photon.* **2009**, *1*, 162−235.
(44) Yan, R.; Gargas, D.; Yang, P. Nanowire photonics. *Nat. Photonics* **2009**, *3*, 569−576.
(45) Leuthold, J.; Koos, C.; Freude, W. Nonlinear silicon photonics. *Nat. Photonics* **2010**, *4*, 535−544.
(46) Almeida, V. R.; Barrios, C. A.; Panepucci, R. R.; Lipson, M. All-optical control of light on a silicon chip. *Nature* **2004**, *431*, 1081−1084.
(47) Daniel, B. A.; Agrawal, G. P. Dependence of dispersive and birefringence properties of silicon nanowires on waveguide dimensions. *Opt. Lett.* **2010**, *35*, 190−192.
(48) Palik, E. D., Ed. *Handbook of Optical Constants of Solids*; Academic Press, 1985.
(49) Malitson, I. H. Interspecimen comparison of the refractive index of fused silica. *J. Opt. Soc. Am.* **1965**, *55*, 1205−1208.
(50) Dulkeith, E.; Xia, F.; Schares, L.; Green, W. M. J.; Vlasov, Y. A. Group index and group velocity dispersion in silicon-on-insulator photonic wires. *Opt. Express* **2006**, *14*, 3853−3863.
(51) Jágerská, J.; Le Thomas, N.; Houdré, R.; Bolten, J.; Moormann, C.; Wahlbrink, T.; Čtyroký, J.; Waldow, M.; Först, M. Dispersion properties of silicon nanophotonic waveguides investigated with Fourier optics. *Opt. Lett.* **2007**, *32*, 2723−2725.
(52) Turner, A. C.; Manolatou, C.; Schmidt, B. S.; Lipson, M.; Foster, M. A.; Sharping, J. E.; Gaeta, A. L. Tailored anomalous group-velocity dispersion in silicon channel waveguides. *Opt. Express* **2006**, *14*, 4357−4362.
(53) Agrawal, G. P. *Nonlinear Fiber Optics*; Academic Press, 2001.
(54) Wulf, M.; Beggs, D. M.; Rotenberg, N.; Kuipers, L. Unravelling nonlinear spectral evolution using nanoscale photonic near-field point-to-point measurements. *Nano Lett.* **2013**, *13*, 5858−5865.
(55) Steinberger, B.; Hohenau, A.; Ditlbacher, H.; Stepanov, A. L.; Drezet, A.; Aussenegg, F. R.; Leitner, A.; Krenn, J. R. Dielectric stripes on gold as surface plasmon waveguides. *Appl. Phys. Lett.* **2006**, *88*, 094104.